Quantum Harmonic Oscillator Spectrum Analyzers

Jonas Keller,[1,2,*] Pan-Yu Hou,[1,2] Katherine C. McCormick,[1,2,†] Daniel C. Cole,[1] Stephen D. Erickson,[1,2] Jenny J. Wu,[1,2] Andrew C. Wilson,[1] and Dietrich Leibfried[1]
[1]National Institute of Standards and Technology, 325 Broadway, Boulder, Colorado 80305, USA
[2]Department of Physics, University of Colorado, Boulder, Colorado 80309, USA

(Received 20 October 2020; accepted 8 April 2021; published 25 June 2021)

Characterization and suppression of noise are essential for the control of harmonic oscillators in the quantum regime. We measure the noise spectrum of a quantum harmonic oscillator from low frequency to near the oscillator resonance by sensing its response to amplitude modulated periodic drives with a qubit. Using the motion of a trapped ion, we experimentally demonstrate two different implementations with combined sensitivity to noise from 500 Hz to 600 kHz. We apply our method to measure the intrinsic noise spectrum of an ion trap potential in a previously unaccessed frequency range.

DOI: 10.1103/PhysRevLett.126.250507

Harmonic oscillators (HOs) are ubiquitous in physics, describing such diverse phenomena as molecular vibrations, the baryon acoustic oscillations in the early Universe [1], electromagnetic fields, and normal or superconducting electrical circuits. Some HO systems—for example microresonators [2], the motion of neutral atoms [3] and ions [4] in trapping potentials, photons in optical and microwave resonators [5], and vibrations in solids [6,7]—can be controlled in the quantum regime. Precisely controlled HO systems feature prominently in precision metrology [8], fundamental quantum mechanical research [5], and quantum information processing (QIP) [9]. QIP uses quantum-controlled HO degrees of freedom either as units of quantum information in their own right [10–12] or as a mechanism to couple identical [2,13,14] or distinct quantum bits (qubits) [15–18]. In all instances, noise limits the practical coherence of HOs, which makes proper noise characterization desirable.

For two-level systems, techniques pioneered in the field of nuclear magnetic resonance [such as the Hahn echo [19] and Carr-Purcell-Meiboom-Gill (CPMG) sequences [20,21]] as well as dynamical decoupling [22] and adaptations [23,24], are routinely employed to suppress sensitivity to noise at certain frequencies or to characterize its spectrum [25–29]. Here, we apply similar principles to an HO and make use of its larger Hilbert space to simplify spectrum reconstruction and remove ambiguities. We demonstrate two different methods experimentally with a trapped ion and explore previously unaccessed regions of its motional spectrum. Manipulation and readout of the HO state is achieved in our case via a Jaynes-Cummings (JC) type coupling to a qubit [30]. This concept can be applied in other HO systems as well, and experimental capabilities suitable for our techniques have been demonstrated, e.g., with microwave [31] and acoustic [32] resonators.

We would like to link fluctuations $\Delta(t)$ of the HO's angular frequency over time t, which we assume to be ergodic and stationary, to a time-independent, two-sided power-spectral density (PSD) $S_\Delta(f)$. For infinite time resolution and sampling duration, $S_\Delta(f)$ can be obtained from a time series record of $\Delta(t) = \omega(t) - \omega_0$, referenced to a local oscillator (LO) at ω_0, as the Fourier transform of the autocorrelation function of $\Delta(t)$. In practical frequency analysis with finite time resolution and sampling duration, a filter $\tilde{s}(f)$ typically removes frequency contributions to $S_\Delta(f)$ outside a band of interest around a center frequency f_0. Popular choices are Gaussian or Blackman [33] filters of a certain width δf. The chosen filter can be related to a sensitivity function $s(t)$ applied to $\Delta(t)$ by [34,35]

$$\langle \phi^2 \rangle := \int_{-\infty}^{\infty} |\tilde{s}(f)|^2 S_\Delta(f) df = \left\langle \left| \int_{-t_w}^{t_w} s(t)\Delta(t) dt \right|^2 \right\rangle, \tag{1}$$

where $\langle \phi^2 \rangle$ is proportional to the spectral power inside the filter, $s(t)$ is the Fourier transform of $\tilde{s}(f)$ and the measurement duration $2t_w$ has to be chosen such that $s(t)$ approximately vanishes outside $[-t_w, t_w]$. The physical meaning of the quantity ϕ depends on the implementation. For a resolution bandwidth of δ_{rbw}, defined here as the full width at half maximum (FWHM) of $|\tilde{s}(f)|^2$, we define the amplification $a_{\tilde{s}}$ as

$$a_{\tilde{s}} := \left(\int_{-\infty}^{\infty} |\tilde{s}(f)|^2 df \right) / \delta_{\mathrm{rbw}}, \tag{2}$$

and approximate the PSD around f_0, filtered by $\tilde{s}(f)$, by

$$\tilde{S}_\Delta(f_0) = \langle \phi^2 \rangle / (a_{\tilde{s}} \delta_{\mathrm{rbw}}). \tag{3}$$

For $\delta_{\mathrm{rbw}} \to 0$, $\tilde{S}_\Delta(f)$ approaches $S_\Delta(f)$.

Smoothly varying envelopes $s(t)$ can suppress side lobes and harmonics in $|\tilde{s}(f)|^2$ and thus simplify the interpretation of $\tilde{S}_\Delta(f)$ and the approximate reconstruction of $S_\Delta(f)$. We apply this principle to two techniques we have previously demonstrated with square-wave filters: $s(t)$ is either implemented by coherently driving the HO [38], or it is approximated by a function with discrete steps for which we prepare different number states of the HO [39]. While the discrete approximation requires more experimental control—in our case provided by the JC coupling to a qubit—it can realize the same amplification $a_{\tilde{s}}$ with states of lower average energy compared to the realization based on coherent driving [39]. The two other capabilities required by both methods are enabled by JC coupling as well: Initialization of the HO in its ground state, and a second-order readout process $f(\phi) \propto \phi^2$ that determines the noise power via the second moment $\langle \phi^2 \rangle \propto \langle f(\phi) \rangle$ of the respective linear HO response ϕ.

Coherent displacements of the HO state are frequently implemented with a resonant force due to a classical field [40]. A force resonant with the LO frequency ω_0 results in the Hamiltonian

$$H_d(t) = -2\hbar\Omega_d(t)(a + a^\dagger)\sin(\omega_0 t). \tag{4}$$

We use the time-dependent drive amplitude $\Omega_d(t)$ to define the filter function $s(t)$. When initialized in the ground state, the HO remains in a coherent state $|\alpha(t)\rangle$ under the influence of the drive Eq. (4) and fluctuations $\Delta(t)$. In the LO reference frame, $\alpha(t)$ obeys the equation of motion [35]

$$\dot{\alpha}(t) = \Omega_d(t) - i\alpha(t)\Delta(t). \tag{5}$$

Integrating Eq. (5) in the absence of noise ($\Delta(t) = 0$) leads to a trajectory $\alpha_0(t)$ that takes real values at all times. With a drive amplitude $\Omega_d(t) = \dot{s}(t)$, the boundary conditions $\alpha_0(-t_w) = \alpha_0(t_w) \simeq 0$ hold and the displacement $\alpha_0(t) = s(t)$ can act as a sensitivity function. Figure 1(a) shows an example for $\Omega_d(t)$ and its associated displacement pattern $\alpha_0(t)$, which is a sinusoidal oscillation inside a Blackman envelope.

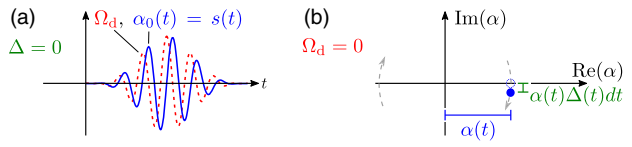

FIG. 1. Implementation of filter functions $s(t)$ using coherent displacements. (a) In the absence of noise [$\Delta(t) = 0$], the time-dependent displacement $\alpha_0(t)$ along the real axis (solid line) is proportional to the integral over time of the coherent drive $\Omega_d(t)$ (dashed line). (b) In the LO reference frame rotating at ω_0, frequency fluctuations $\Delta(t)$ cause azimuthal rotations. During an infinitesimal time step dt, this produces a displacement perpendicular to $\alpha(t)$ and equal to $-i\alpha(t)\Delta(t)dt$. For small rotations, $\mathrm{Re}[\alpha(t)] \approx \alpha_0(t)$ thus controls the sensitivity to $\Delta(t)$ and implements a filter function $s(t)$.

Fluctuations of the HO frequency produce additional displacements. As illustrated in Fig. 1(b), the noisy HO rotates relative to the LO with angular velocity $\Delta(t)$, which leads to displacements at a rate $-i\alpha(t)\Delta(t)$, proportional to the distance from the origin and perpendicular to $\alpha(t)$. For small angles, $|\int_{-t_w}^{t} \Delta(\tau)d\tau| \ll 1 \;\; \forall \;\; t \in [-t_w, t_w]$, the rotational character of these displacements can be neglected, i.e., $i\alpha(t)\Delta(t)dt \approx i\alpha_0(t)\Delta(t)dt$. In this approximation, the total displacement at the end of the sequence is [35]

$$\alpha(t_w) \approx -i\int_{-t_w}^{t_w} \alpha_0(t)\Delta(t)dt, \tag{6}$$

such that $\langle |\alpha(t_w)|^2 \rangle =: \langle \phi^2 \rangle$ is proportional to the noise power within $\tilde{s}(f)$ according to Eq. (1). If the small-angle approximation is violated, higher-order terms in the noise power modify the spectral sensitivity [35]. We detect $|\alpha(t_w)|^2$ via the probability of a spin flip when driving a motion-subtracting sideband of the coupled qubit-HO system [35,38,41,42]. This method relies on the fact that the transition is forbidden when the HO is in its ground state, and the spin flip probability is proportional to $|\alpha|^2$ for small displacements (to within 5% as long as $|\alpha| < 0.47$ for the experimental parameters used below [35]).

Alternatively, the sensitivity function can be approximated in discrete steps by preparing superpositions of number states [39]

$$|\Psi_{n_1,n_2}(t)\rangle = \frac{1}{\sqrt{2}}(|n_1\rangle + e^{i\phi(t)}|n_2\rangle), \tag{7}$$

where $|n_i\rangle$ is the number state with n_i phonons. In the interaction picture rotating with the LO, the instantaneous energy shifts of the two components are $E_i(t) = \hbar n_i \Delta(t)$, which leads to a time dependence of the relative phase described by

$$\phi(t) = \phi(t_0) + \int_{t_0}^{t} (n_1 - n_2)\Delta(\tau)d\tau. \tag{8}$$

The rate at which ϕ accumulates is proportional to $\Delta(t)$ and scaled by $\delta n = (n_1 - n_2)$. By incrementing and decrementing n_i, we can produce a sensitivity function $s(t) \coloneqq \delta n(t)$ with discrete steps as illustrated in Fig. 2(a) for the example of a sinusoid within a Hann window [34]. Figure 2(b) shows the respective frequency domain filter function $\tilde{s}(f)$. Manipulation of the motional state can be achieved via sideband transitions in the qubit-HO system [35,39,43]: Analogous to a Ramsey sequence, a $\pi/2$ sideband pulse transfers the system from its initial pure state into a superposition. Subsequent increments and decrements of δn shape $s(t)$. To prepare superposition components

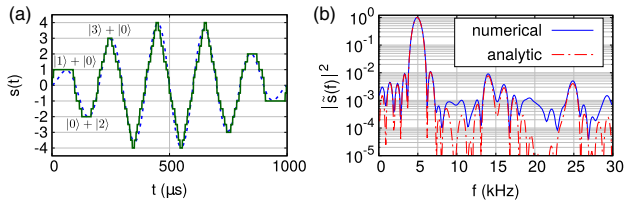

FIG. 2. Implementation of filter functions $s(t)$ using number state superpositions. (a) Sensitivity function approximating a Hann filter (dashed line) by a piecewise constant sensitivity $s(t) = n_1 - n_2$ (solid line) in different superpositions of number states $|n_1\rangle$ and $|n_2\rangle$, as indicated by the labels [cf. Eq. (7); phase and normalization omitted for clarity]. (b) The filter $|\tilde{s}(f)|^2$ corresponding to $s(t)$ shown in (a), calculated both analytically using a simple model and numerically [35].

beyond $n_i = 2$, our scheme requires a three-level system in place of the qubit. At the end of the sequence, a $\pi/2$ sideband pulse maps the relative phase ϕ onto the qubit state populations for readout.

We demonstrate both methods experimentally with the axial harmonic motion of a single $^9Be^+$ ion in a linear Paul trap. The coherent displacement experiments use the room-temperature, wafer-based, 3D trap described in Ref. [44], while the number state superposition method is demonstrated in a cryogenic surface-electrode trap (see Ref. [45]). The distances between the ion and the nearest electrode are 160 and 40 μm, and the axial motion is heated at a rate of ca. 160 and 20 phonons/ sec under the respective operating conditions.

Implementation with coherent displacements.—At the start of each experiment, the axial secular motion of the ion at $\omega_0 \approx 2\pi \times 3.5$ MHz is initialized in its ground state via resolved sideband cooling. The voltage on a nearby electrode is modulated to produce an electric field that realizes the coherent drive of Eq. (4). This modulation consists of a carrier signal at the LO frequency ω_0 with an amplitude modulation $\propto \Omega_d(t)$, determined by the derivative of the desired sensitivity function $\alpha_0(t) = s(t)$. Our choice of a sinusoid under a Blackman envelope, with total duration $2t_w$ and k oscillations within t_w, results in a filter function $\tilde{s}(f)$ centered around $f_0 = k/t_w$, with bandwidth $\delta_{\mathrm{rbw}} \approx 0.822/t_\omega$ [35]. The final motional state is mapped onto internal states as described above and detected via state-dependent fluorescence. For the purpose of filter characterization, we use another dc electrode to apply an oscillating electric potential curvature as synthetic noise,

$$\Delta_{\mathrm{test}}(t) = \Delta_0 \cos(2\pi f_{\mathrm{noise}} t + \varphi), \tag{9}$$

with a constant amplitude Δ_0 and a random phase φ with respect to $s(t)$.

Figure 3(a) shows the response to a modulation $\Delta_{\mathrm{test}}(t)$ with $\Delta_0 = 2\pi \times 55$ Hz at the center frequency of the filter, $f_{\mathrm{noise}} = 8$ kHz $= k/t_w$ (where $k = 2$ and $t_w = 250$ μs), as a function of the filter amplitude. Δ_0 is determined from the fit of a theoretical model (solid line), which includes a separately determined finite thermal energy of 0.055 $\hbar\omega_0$ due to imperfect state preparation and heating during the sequence. The initial monotonic range of this response can

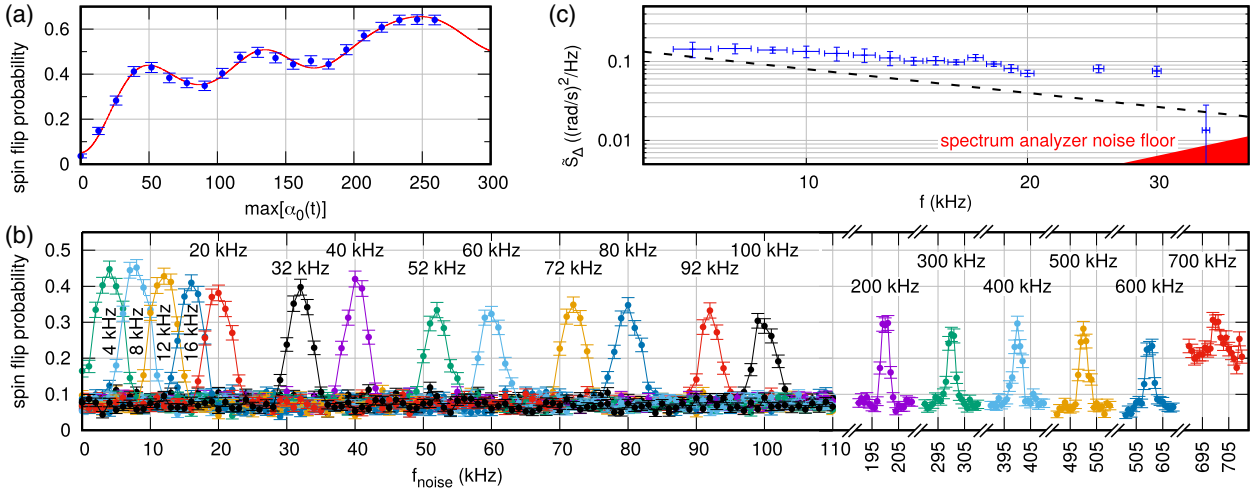

FIG. 3. Experimental results of the coherent displacement method. (a) Response to a $f_{\mathrm{noise}} = f_0 = 8$ kHz sinusoidal modulation of the HO frequency as a function of the filter amplification (symbols: experimental data, line: model with the modulation amplitude Δ_0 as a free parameter). (b) Measured response of various filter functions ($t_w = 250$ μs, varied k) to sinusoidal modulations of varied frequency and random phase. The modulation amplitude Δ_0 and filter amplification are chosen to keep the signal within the first monotonic increase of the function shown in (a). Filter functions above 100 kHz are measured with increased modulation to compensate technical limitations of the filter amplitude in this regime. Data points are linked with solid lines to guide the eye. (c) Power spectral density estimate of the HO frequency noise, determined from the transmission through filter functions with $t_w = 1$ ms and varied k. The dashed line indicates a $1/f$ slope to guide the eye. Experimental data in all subfigures are averages over 200 repetitions. Error bars: 1σ (vertical), δ_{rbw} [horizontal in (c)].

be used to measure the spectral sensitivity of a filter function by varying the modulation frequency f_{noise}, as demonstrated in Fig. 3(b). We implement filter functions with $t_w = 250$ μs and different values of k, centered around $k \times 4$ kHz. For data up to $f_0 = 100$ kHz, the filter and modulation amplitudes are nominally kept constant at $\Delta_0 \approx 2\pi \times 300$ kHz and $\max[\alpha_0(t)] = 10$ throughout the measurement. We attribute signal decrease with increasing filter frequencies to a reduction of Δ_0 due to imperfect compensation of the low-pass filter through which the modulation is applied. The drive Ω_d required to achieve a given filter amplification $a_{\tilde{s}} \propto \max[\alpha_0(t)]$ increases linearly with f_0. We apply a rather conservative limit to the drive voltage due to unknown damage thresholds of integrated filter components, resulting in $|\Omega_d| \leq 2\pi \times 2.1$ MHz, which corresponds to an electric field of $E_d \leq 1.37\mathrm{V/m}$ at the ion position. To observe filter functions at center frequencies above $f_0 = 100$ kHz, we instead increase the modulation amplitude Δ_0. These data demonstrate the implementation of filter functions up to $f_0 = 600$ kHz ($t_w = 250$ μs, $k = 150$). For $f_0 = 700$ kHz, we observe a significant increase of the background, i.e., a displacement $\alpha(t_w)$ that is independent of $\Delta(t)$, likely due to an increased sensitivity to deviations of $\Omega_d(t)$ from its ideal shape.

Figure 3(c) shows an experimentally determined estimate of the trap frequency noise PSD using Eq. (3) and filter functions with $t_w = 1$ ms and $k = 7 \ldots 35$ (see Supplemental Material [35] for evaluation details). It might be interpreted as localized features, e.g., around 30 kHz, on top of a $1/f$ trend (as indicated by the dashed line), as often found in technical noise sources and some models of electric field noise near surfaces [46]. Distinct features might be caused by specific devices in the experimental setup. In this case the spectrum analysis could aid in suppressing such contributions and further measurements focused on these regions can document improvements. In the following, we assess the frequency span and dynamic range of our implementation. The upper bound of the dynamic range is set by the linearity condition for the noise amplitude ($|\int_{-t_w}^{t} \Delta(\tau) d\tau| \ll 1$, see above). The lowest detectable noise power is determined by shot noise and the obtainable filter amplification, which decreases linearly with f_0 for limited Ω_d. In the above example with $t_w = 1$ ms, it is $\tilde{S}_{\Delta,\mathrm{min}} \approx 7.1 \times 10^{-12}\ (\mathrm{rad/s})^2/\mathrm{Hz}^3 \times f_0^2$ [35], as indicated by the shaded area in Fig. 3(c). Finite temperature, e.g., due to imperfect initialization or heating during the sequence, reduces detection contrast and thus increases the noise floor [35]. If necessary, this limit can be reduced by averaging over more repetitions or higher amplification. The lower end of the frequency span is close to the minimum resolution bandwidth, which is determined by the maximum sequence duration with acceptable heating of the ion motion. The highest filter function frequency is limited by amplitude noise and distortion of fast drive waveforms Ω_d. Since the evolution according to Eq. (5) displaces the wave function without deformation, the readout signal could be increased by choosing a different initial state. Using number states with $n \geq 1$ in place of the ground state would result in a quantum-enhanced displacement sensitivity [35,43,47].

Implementation with number state superpositions.—Motional state superpositions are generated using optical Raman and microwave transitions between states within the ${}^2S_{1/2}$ manifold [35,39]. The phase ϕ is read out by mapping the superposition phase onto the qubit state populations, followed by a projective measurement using fluorescence detection. The resulting signal,

$$P_{\mathrm{bright}} = \sin^2\left(\frac{\phi}{2}\right) = \frac{\phi^2}{4} + \mathcal{O}(\phi^4), \tag{10}$$

provides the required ϕ^2 dependence of a noise power measurement if a sufficiently small overall phase $|\phi| \ll \pi/2$ is obtained at the end of the sequence.

We again observe the spectral sensitivities of the filter functions via sinusoidal modulation of the HO frequency, cf. Eq. (9). The result is shown in Fig. 4 for ten different filter functions between 500 Hz and 5 kHz. The upper limit of this frequency range, as well as the maximum sensitivity $|\delta n|$ for a given filter frequency, are determined by the pulse times needed to switch between superpositions, i.e., by the achievable Raman Rabi frequencies. The minimum frequency and bandwidth decrease with longer sequence durations. In the presence of heating, this presents a similar trade-off with the signal-to-noise ratio as for the coherent displacement method.

Summary and conclusions.—We have introduced a technique to measure the spectral composition of frequency fluctuations in harmonic oscillators in the quantum regime. Using a single trapped ion, we have demonstrated two

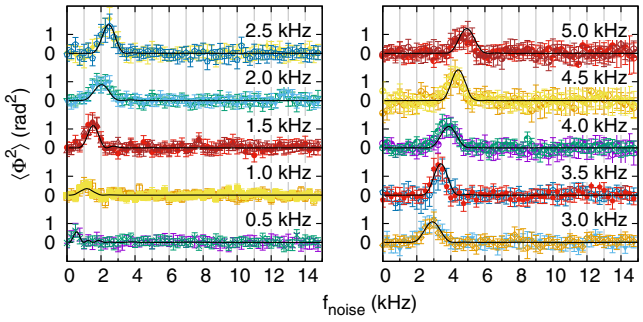

FIG. 4. Number state implementation results: Measured response of different filter functions to applied modulation of varied frequency f_{noise} and random phase. The 5.0 kHz trace corresponds to the sensitivity function in Fig. 2. The solid lines show the expected response, adjusted by a global scaling factor to account for the dependence of the modulation depth on the applied voltage. Each data point represents 200 repetitions, error bars: 1σ.

different implementations. The first is based on coherent driving with a resonant force and thus simple to apply. Its signals consist of a phase-space displacement proportional to the noise power within the filter, which we measure via the coupling to a two-level system. The method may also be applicable if the HO is naturally found in the ground state and the average occupation can be read out by other means than a sideband interaction. We have shown the coverage of a span from 4 to 600 kHz with filter functions of 4 kHz resolution bandwidth using externally applied modulations as test signals. A measurement of the electric potential noise in our ion trap was performed between 7 and 35 kHz, limited by a conservative amplification restriction due to unknown component damage thresholds. The second method uses a sequence of different number state superpositions that acquire a phase difference in the presence of noise, which we read out by mapping it onto a qubit. While this method requires more advanced control over the motional state, its sensitivity scales more favorably—linearly as opposed to $\propto \sqrt{E_{\max}}$—with the maximum energy $E_{\max}$ of the HO. We have generated such filter functions ranging from 500 Hz to 5 kHz, with the maximum frequency limited by the minimal duration of our number state manipulations.

These methods can be applied to any quantum harmonic oscillator for which the respective experimental capabilities for motional state manipulation and readout exist. In trapped ions, they extend the spectral range over which fluctuations of the motional frequency can be measured. This can enable better understanding and improvement of two-qubit gate fidelities [48,49] and provide new insights into electric field noise from nearby electrode surfaces and the resulting anomalous heating [46].

A complementary approach using Schrödinger cat states has recently been demonstrated in [50].

We thank D. R. Leibrandt and J. F. Niedermeyer for a careful reading of the manuscript, and D. H. Slichter for helpful advice and discussions. At the time the work was performed, J. K., P.-Y. H., K. C. M., S. D. E., and J. J. W. were Associates in the Professional Research Experience Program (PREP) operated jointly by NIST and the University of Colorado under award 70NANB18H006 from the U.S. Department of Commerce, National Institute of Standards and Technology. This work was supported by the NIST Quantum Information Program and IARPA. J. K. acknowledges support by the Alexander von Humboldt Foundation. K. C. M. acknowledges support by an ARO QuaCGR fellowship through Grant No. W911NF-14-1-0079. D. C. C. is supported by a National Research Council postdoctoral fellowship. S. D. E. acknowledges support from the National Science Foundation under Grant No. DGE 1650115. Numerical calculations were performed using QuTiP [51]. The experiments were performed using the ARTIQ control system. This Letter is a contribution of NIST, not subject to U.S. copyright.

*Present Address: Physikalisch-Technische Bundesanstalt, Bundesallee 100, 38116 Braunschweig, Germany.
†Present Address: Department of Physics, University of Washington, Seattle, Washington 98195, USA.

[1] D. J. Eisenstein *et al.*, Astrophys. J. **633**, 560 (2005).
[2] M. Aspelmeyer, T. J. Kippenberg, and F. Marquardt, Rev. Mod. Phys. **86**, 1391 (2014).
[3] R. Grimm, M. Weidemüller, and Y. B. Ovchinnikov, *Optical Dipole Traps for Neutral Atoms* (Academic Press, New York, 2000), p. 95.
[4] D. Leibfried, R. Blatt, C. Monroe, and D. J. Wineland, Rev. Mod. Phys. **75**, 281 (2003).
[5] S. Haroche and J.-M. Raymond, *Exploring the Quantum* (Oxford University Press, Oxford, UK, 2006).
[6] K. C. Lee, M. R. Sprague, B. J. Sussman, J. Nunn, N. K. Langford, X. M. Jin, T. Champion, P. Michelberger, K. F. Reim, D. England, D. Jaksch, and I. A. Walmsley, Science **334**, 1253 (2011).
[7] P. Y. Hou, Y. Y. Huang, X. X. Yuan, X. Y. Chang, C. Zu, L. He, and L. M. Duan, Nat. Commun. **7**, 11736 (2016).
[8] J. Aasi *et al.*, Nat. Photonics **7**, 613 (2013).
[9] T. D. Ladd, F. Jelezko, R. Laflamme, Y. Nakamura, C. Monroe, and J. L. O'Brien, Nature (London) **464**, 45 (2010).
[10] D. Gottesman, A. Kitaev, and J. Preskill, Phys. Rev. A **64**, 012310 (2001).
[11] C. Flühmann, T. L. Nguyen, M. Marinelli, V. Negnevitsky, K. Mehta, and J. P. Home, Nature (London) **566**, 513 (2019).
[12] P. Campagne-Ibarcq, A. Eickbusch, S. Touzard, E. Zalys-Geller, N. E. Frattini, V. V. Sivak, P. Reinhold, S. Puri, S. Shankar, R. J. Schoelkopf, L. Frunzio, M. Mirrahimi, and M. H. Devoret, Nature (London) **584**, 368 (2020).
[13] J. I. Cirac and P. Zoller, Phys. Rev. Lett. **74**, 4091 (1995).
[14] A. Blais, R.-S. Huang, A. Wallraff, S. M. Girvin, and R. J. Schoelkopf, Phys. Rev. A **69**, 062320 (2004).
[15] Z.-L. Xiang, S. Ashhab, J. Q. You, and F. Nori, Rev. Mod. Phys. **85**, 623 (2013).
[16] R. W. Andrews, R. W. Peterson, T. P. Purdy, K. Cicak, R. W. Simmonds, C. A. Regal, and K. W. Lehnert, Nat. Phys. **10**, 321 (2014).
[17] G. Kurizki, P. Bertet, Y. Kubo, K. Mølmer, D. Petrosyan, P. Rabl, and J. Schmiedmayer, Proc. Natl. Acad. Sci. U.S.A. **112**, 3866 (2015).
[18] S. Kotler, R. W. Simmonds, D. Leibfried, and D. J. Wineland, Phys. Rev. A **95**, 022327 (2017).
[19] E. L. Hahn, Phys. Rev. **80**, 580 (1950).
[20] H. Y. Carr and E. M. Purcell, Phys. Rev. **94**, 630 (1954).
[21] S. Meiboom and D. Gill, Rev. Sci. Instrum. **29**, 688 (1958).
[22] L. Viola, E. Knill, and S. Lloyd, Phys. Rev. Lett. **82**, 2417 (1999).
[23] G. S. Uhrig, Phys. Rev. Lett. **98**, 100504 (2007).
[24] M. J. Biercuk, H. Uys, A. P. Vandevender, N. Shiga, W. M. Itano, and J. J. Bollinger, Nature (London) **458**, 996 (2009).
[25] S. Lasič, J. Stepišnik, and A. Mohorič, J. Magn. Reson. **182**, 208 (2006).
[26] G. A. Álvarez and D. Suter, Phys. Rev. Lett. **107**, 230501 (2011).
[27] J. Bylander, S. Gustavsson, F. Yan, F. Yoshihara, K. Harrabi, G. Fitch, D. G. Cory, Y. Nakamura, J.-S. Tsai, and W. D. Oliver, Nat. Phys. **7**, 565 (2011).

[28] S. Kotler, N. Akerman, Y. Glickman, and R. Ozeri, Phys. Rev. Lett. **110**, 110503 (2013).
[29] M. Bishof, X. Zhang, M. J. Martin, and J. Ye, Phys. Rev. Lett. **111**, 093604 (2013).
[30] C. A. Blockley, D. F. Walls, and H. Risken, Europhys. Lett. **17**, 509 (1992).
[31] M. Hofheinz, H. Wang, M. Ansmann, R. C. Bialczak, E. Lucero, M. Neeley, A. D. O'Connell, D. Sank, J. Wenner, J. M. Martinis, and A. N. Cleland, Nature (London) **459**, 546 (2009).
[32] Y. Chu, P. Kharel, T. Yoon, L. Frunzio, P. T. Rakich, and R. J. Schoelkopf, Nature (London) **563**, 666 (2018).
[33] R. B. Blackman and J. W. Tukey, Bell Syst. Tech. J. **37**, 485 (1958).
[34] R. B. Blackman and J. W. Tukey, Bell Syst. Tech. J. **37**, 185 (1958).
[35] See Supplemental Material at http://link.aps.org/supplemental/10.1103/PhysRevLett.126.250507 for derivations and experimental details, which includes Refs. [36,37].
[36] M. Suzuki, Proc. Jpn. Acad. **69**, 161 (1993).
[37] R. Bowler, U. Warring, J. W. Britton, B. C. Sawyer, and J. Amini, Rev. Sci. Instrum. **84**, 033108 (2013).
[38] K. C. McCormick, J. Keller, D. J. Wineland, A. C. Wilson, and D. Leibfried, Quantum Sci. Technol. **4**, 024010 (2019).
[39] K. C. McCormick, J. Keller, S. C. Burd, D. J. Wineland, A. C. Wilson, and D. Leibfried, Nature (London) **572**, 86 (2019).
[40] P. Carruthers and M. M. Nieto, Am. J. Phys. **33**, 537 (1965).
[41] D. J. Wineland, C. Monroe, W. M. Itano, D. Leibfried, B. E. King, and D. M. Meekhof, J. Res. Natl. Inst. Stand. Technol. **103**, 259 (1998).
[42] J. P. Home, D. Hanneke, J. D. Jost, D. Leibfried, and D. J. Wineland, New J. Phys. **13**, 073026 (2011).
[43] K. C. McCormick, Control and measurement of a single-ion quantum harmonic oscillator, Ph.D. thesis, University of Colorado Boulder, 2019.
[44] R. B. Blakestad, C. Ospelkaus, A. P. VanDevender, J. M. Amini, J. Britton, D. Leibfried, and D. J. Wineland, Phys. Rev. Lett. **102**, 153002 (2009).
[45] K. R. Brown, C. Ospelkaus, Y. Colombe, A. C. Wilson, D. Leibfried, and D. J. Wineland, Nature (London) **471**, 196 (2011).
[46] M. Brownnutt, M. Kumph, P. Rabl, and R. Blatt, Rev. Mod. Phys. **87**, 1419 (2015).
[47] F. Wolf, C. Shi, J. C. Heip, M. Gessner, L. Pezzè, A. Smerzi, M. Schulte, K. Hammerer, and P. O. Schmidt, Nat. Commun. **10**, 2929 (2019).
[48] I. Talukdar, D. J. Gorman, N. Daniilidis, P. Schindler, S. Ebadi, H. Kaufmann, T. Zhang, and H. Häffner, Phys. Rev. A **93**, 043415 (2016).
[49] A. R. Milne, C. L. Edmunds, C. Hempel, F. Roy, S. Mavadia, and M. J. Biercuk, Phys. Rev. Applied **13**, 024022 (2020).
[50] A. R. Milne, C. Hempel, L. Li, C. L. Edmunds, H. J. Slatyer, H. Ball, M. R. Hush, and M. J. Biercuk, preceding Letter, Phys. Rev. Lett. **126**, 250506 (2021).
[51] J. R. Johansson, P. D. Nation, and F. Nori, Comput. Phys. Commun. **184**, 1234 (2013).